Journal of Applied Research and Technology

www.jart.icat.unam.mx

Instituto de Ciencias Aplicadas y Tecnología

Journal of Applied Research and Technology 24 (2026) 598-609

Original

Assessing Fine Particulate Matter ($PM_{2.5}$) Pedestrian Exposure in Urban Environments: Low-Cost Sensor Deployment and Preliminary Findings in Puebla's Historic Center

Marco Antonio Mora-Ramírez*[1] • Tomás Carrasco Fuentes[2]
Xóchitl Cruz Núñez[3] • Carmen Cerón Garnica[4]

[1]Laboratorio Universitario de Calidad del Aire, Facultad de Ciencias Químicas, Benemérita Universidad Autónoma de Puebla.
[2]Facultad de Ciencias de la Electrónica, Benemérita Universidad Autónoma de Puebla.
[3]Instituto de Ciencias de la Atmósfera y Cambio Climático, Universidad Nacional Autónoma de México, Coyoacán, 04510 Ciudad de México, CDMX.
[4]Facultad de Ciencias de la Computación, Benemérita Universidad Autónoma de Puebla.

Received: 12 03 2025; Accepted: 03 07 2025
Available: 31 08 2026

Abstract: In urban areas, people are systematically exposed to fine particulate matter ($PM_{2.5}$) while commuting or engaging in public activities. Therefore, it is crucial to use devices for measuring $PM_{2.5}$. Low-cost sensors (LCS) are an emerging technology with the potential to enable accurate measurements at a fraction of the cost and on a mobile platform. This study provides insights into the construction, programming, and calibration of LCS-equipped devices, along with the initial findings from pedestrian measurements on streets and avenues in the historic center of Puebla. The results show that, in addition to vehicle emissions, the resuspension of particulate matter by automobiles at pedestrian crossings is an essential factor for $PM_{2.5}$ exposure among individuals who halt at traffic lights. $PM_{2.5}$ levels in several areas of Puebla City's historic center exceed permitted levels, underscoring the importance of this research for public health.

Keywords: **Low-cost sensors, $PM_{2.5}$, pedestrian exposure, air quality, mobile measurements**

*Corresponding author.
E-mail address: marco.morar@correo.buap.mx (M.A. Mora-Ramírez).
Peer Review under the responsibility of Universidad Nacional Autónoma de México.

1. Introduction

Fine particulate matter (i.e., particulate matter with aerodynamic diameter less than 2.5 µm) ($PM_{2.5}$) poses a serious public health risk as it can enter the circulatory system and accumulate in various body organs (Thangavel et al., 2022). In urban areas, $PM_{2.5}$ is emitted from diesel vehicles, fossil fuel burning, industrial activities, biomass burning, and airborne dust.

To effectively measure $PM_{2.5}$ exposure and mitigate its effects, local governments worldwide must systematically measure ambient $PM_{2.5}$ levels. However, the widespread use of fixed monitoring stations is constrained by significant installation, operation, and maintenance costs, particularly in low- and middle-income countries (Cromar et al., 2019; Desouza et al., 2020). Moreover, fixed monitoring sites can only provide representative data within a radius of up to 3 km and are generally unable to detect high concentrations or sudden changes, unlike mobile monitoring equipped with low-cost sensors (LCS) (Khreis et al., 2022; Pang et al., 2021).

LCS is an emerging technology for assessing pedestrian exposure to air pollution on urban roads. They offer valuable information to improve public understanding and communication of air quality (Feenstra, 2020; Gao et al., 2015; Lee et al., 2019; Liu et al., 2020), especially for those with health concerns, such as asthma, wheezing, and seasonal allergies (Raysoni et al., 2023), and in air quality planning (Omidvarborna & Kumar, 2024). Likewise, LCS are optical sensors based on the miniaturization of optical particle counters (OPCs) that use light scattering to measure the particle-size distribution of fine particulate matter, according to Mie scattering theory (Ye et al., 2012). Unlike traditional air quality monitoring stations, a mobile LCS network enables dynamic monitoring across the environment and delivers data with unprecedented real-time resolution (Desouza et al., 2020). LCS also enables indoor monitoring applications, outdoor air quality monitoring, emissions monitoring, port and bulk-handling terminal monitoring, mining site monitoring, fence-line monitoring, IT hardware intelligence, contamination hotspot testing, and personal exposure monitoring, among others (WMO, 2024).

The bustling commercial, cultural, and tourist activity in the historical center of Puebla City poses a risk of exposure to elevated $PM_{2.5}$ concentrations exceeding safe levels for pedestrians. In this paper, we introduce the design and set-up of a device equipped with LCS for $PM_{2.5}$, also including temperature, relative humidity, geolocation, time, and data storage/display modules; the design of a protective carcass for personal and outdoor measurements; testing and calibration of devices for accuracy, and results of mobile measurements in the historic center of the city of Puebla to analyze pollutant sources and $PM_{2.5}$ exposure in pedestrian environments.

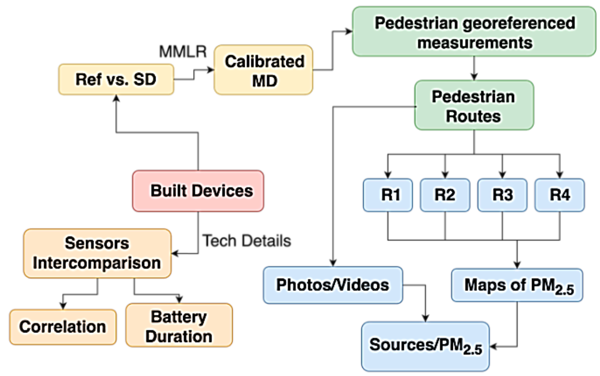

Figure 1. Schematic representation of the research methodology.

2. Materials and Methods

Figure 1 details the study's stages. The process begins with thoroughly documenting the technical specifications for various sensors and electronic components, including GPS, temperature and humidity sensors, particle sensors, a clock, an LCD screen, and a storage module. Next, these components are interlinked, programmed, and appropriately encased. Next, we performed extensive sensor intercomparison tests to evaluate power supply performance and ensure consistent measurements across all devices.

The technical specifications of the sensors offer insights into the performance and functionalities of each component integrated into two devices: the (i) $PM_{2.5}$ Mobile Monitoring Devices (MD) and (ii) $PM_{2.5}$ Static Monitoring Devices (SD). The SD were used to assess reproducibility and for calibration purposes. Calibrated MD were used to perform pedestrian georeferenced measurements along four pre-established routes (R1, R2, R3, and R4). The following sections provide insights into each stage of this project.

2.1 Modules and Sensors

2.1.1 Geolocation

The NEO-6M GPS module in the MD determines precise location using the Global Positioning System (GPS). It enables georeferencing for each measurement captured along the way. Location data is a vital metric for correlating $PM_{2.5}$ measurements with specific environmental conditions within each zone. This enables the identification of areas with higher pollutant concentrations, offering a comprehensive spatial perspective on air quality across locations.

2.1.2 Temperature and Humidity Sensor

The DHT11 sensor measures temperature and relative humidity (RH). It incorporates a thermistor whose resistance changes predictably with temperature. As temperature increases, resistance decreases; as temperature decreases, resistance increases. This change in resistance is directly related to temperature and is converted into a digital signal by an analog-to-digital converter (ADC). The temperature measurement's resolution depends on the digital output's bit depth. When generating humidity data, the DHT11 sensor incorporates a hygrometer that measures the capacitance variation of a metal-oxide polymer as ambient humidity changes (Adhiwibowo et al., 2020). DHT11 sensors are typically factory-calibrated, ensuring they operate within the manufacturer's specified limits. While factory calibration suffices for most applications, manual calibration is an option. This process involves comparing DHT11 readings against those of more precise sensors and applying software offsets to correct temperature and humidity values as necessary. The DHT11 sensor is an ideal choice for applications where high precision is not required, offering an affordable and practical solution. Its minimal maintenance consists of simple tasks, such as cleaning the pins and ensuring the sensor is free of visible damage. Additionally, it should be protected from excessive moisture to maintain optimal performance.

2.1.3 Particulate Matter Sensor ($PM_{2.5}$)

The SDS011 sensor operates by sampling ambient air containing suspended particulate matter, using a fan to draw the air into the sensor. Once inside, the air enters the measurement chamber, where a laser and a photodiode analyze the particulate matter. The laser emits light at specific wavelengths, typically in the near-infrared range. Notably, the SDS011 sensor uses two lasers: one at 650 nm and the other at 780 nm. Such wavelengths are suitable for detecting $PM_{2.5}$ and PM_{10} particles, respectively. The choice of wavelength is critical because it determines how suspended particles interact with light. In the SDS011 sensor, airborne particles scatter the laser light. Two photodiodes, positioned at specific angles relative to the laser beam, measure this scattered light. The first photodiode measures light scattered in a direction that helps estimate the number of larger particles. The second photodiode measures light scattered in another direction, enabling estimation of smaller particles (Nothhelfer et al., 2023). The amount of light correlates with the number and size of particles in the air. By measuring the received light, the sensor can determine the concentration and size distribution of airborne particles. After the photodiodes detect scattered light, the signal-processing phase begins, enabling the SDS011 to provide accurate particulate matter readings. When the microcontroller receives signals from the photodiodes, it uses algorithms and equations based on optical and mathematical principles to calculate the particle concentration in the air.

These calculations establish relationships between scattered light and particle characteristics, translating the amount of scattered light reaching each photodiode into information about particle quantity and size. Once the data has been processed, it is transmitted through a communication interface. This interface is typically digital, with options such as UART, UART-TTL, or USB, enabling seamless communication with devices such as microcontrollers, computers, and monitoring systems (Badura et al., 2018). The data is sent in a specific frame format, which includes headers and checksums to ensure data integrity. The sensor transmits data at configurable regular intervals. In this research, the transmission frequency was set to every 2 seconds. Regular basic maintenance, such as cleaning the air inlet port and protecting the sensor from prolonged exposure to adverse conditions, is crucial to ensure accurate measurements over time. Additionally, according to the manufacturer, the sensor has a specified lifetime of one year. After this period, it is necessary to check or recalibrate the sensor to maintain measurement accuracy. Recalibration can be performed by comparing the sensor readings with those from calibrated reference equipment (Liu et al., 2019).

2.1.4 RTC Module DS3231

To accurately characterize $PM_{2.5}$ concentrations, it is essential to associate each measurement with the specific time (hh:mm) taken. The Real-Time Clock (RTC) module DS3231 provides precise time stamps for each measurement. This module uses a quartz crystal with a stable vibration frequency to generate an accurate signal for time measurement. The crystal pulses are counted in binary, allowing the module to track time in hours, minutes, and seconds (hh:mm:ss), as well as in day, month, and year (dd:MM) formats. Temperature changes can alter the accuracy of time measurements; however, the DS3231 module includes built-in temperature compensation. This circuitry adjusts the clock frequency in response to temperature variations, ensuring consistent measurement quality regardless of thermal changes. Additionally, the module includes a battery backup that maintains accurate timekeeping even when external power is unavailable.

2.1.5 Data Display Interface

The LCD (I2C) display provides a direct interface for viewing real-time data. This allows an immediate review of measurements and provides feedback on air quality at the device's location. In addition, it facilitates adjustments and configuration changes, which are useful during the calibration phase and to ensure that the equipment functions correctly during measurements. The LCD I2C module includes an I2C driver that manages communication between the Arduino and the display. This feature reduces the microcontroller's load and simplifies programming. Several key points should be considered regarding maintenance to ensure optimal data transfer. These include periodically checking the physical connections between the I2C LCD, the PCF8574 converter, and the ATmega328P microprocessor development board to ensure they are properly connected and free of physical damage. It is also essential to keep the associated libraries up to date to ensure compatibility with the latest versions of the Arduino IDE and benefit from potential improvements in performance and stability (Akinwole & Oladimeji, 2018).

2.1.6 Data Storage

In addition to displaying data in real-time, storing all information for later analysis is essential. The microSD module enables recording and storage of all data obtained during measurements. The device facilitates reading and writing data to the microSD memory card using the SPI interface, a synchronous communication protocol that enables fast data transfer between devices. Ensuring that the microSD card reader is connected correctly to the development board and configured for proper SPI communication is essential. The microSD card reader is an excellent choice for projects requiring portable data storage. It offers direct access through the development board and provides a cost-effective, low-power solution. The durability and ease of use of the microSD card make it ideal for standard applications.

2.2 Implementing and Constructing Measuring Devices

Two types of measurement devices were constructed: static devices (SD) and mobile devices (MD). The SDs were designed to be placed outdoors to collect data for sensor calibration. The SD consists of a single development board with an ATmega328P microprocessor, hereinafter referred to as Circuit One (C1). The temperature, humidity, $PM_{2.5}$, microSD, and clock sensors are installed on C1. The MDs are built for georeferenced measurements and are designed to be economical and straightforward for experimental purposes. These devices consist of two circuits. The first circuit corresponds to C1, as described above. The second circuit (C2) includes GPS, clock, display, and data storage modules. Integrating these two circuits (C1 and C2) helps avoid memory saturation and prevents interference between sensors. The development board was programmed using the Arduino Integrated Development Environment (IDE) to implement the sensors and measurement devices. Arduino was selected for its widespread adoption, user-friendly interface, and adaptability to electronics projects. Its extensive developer community provides robust technical support and a wealth of online resources, making it effortless to find examples and solutions for sensor integration.

Programming was executed in the Arduino IDE using the C/C++ programming language native to Arduino. The code was developed to configure and retrieve data from PM2.5 particulate matter, temperature, and relative humidity sensors. Each sensor requires specific libraries to facilitate communication and ensure precise measurements. The sensors are physically connected to the development board via cables or pins to transmit data and power. Each sensor requires specific connections for power, ground, and data, which are identified and linked to corresponding pins on the development board according to the sensor's technical specifications. In addition to sensor integration, a display interface was implemented to visualize data in real-time and facilitate user interaction with the device. The code was designed to present measured values clearly on the screen, enabling users to monitor air quality in real time. A data storage device, such as an SD memory card, was utilized to store the collected data. The code included routines to save measurement values into a log file on the memory card. This allows continuous data storage over time, enabling later analysis and interpretation.

Arduino programming is accessible to individuals with varying levels of programming and electronics experience, facilitating the implementation and development of customized projects such as our low-cost air quality measurement system, thereby enhancing monitoring capabilities in the municipality of Puebla. Detailed reference to the programming lines of code used in both the static measurement device (SD) and the mobile measurement device (MD) is available upon request to the authors of this manuscript. The housing was designed in SolidWorks, enabling 3D modeling to create a virtual representation with detailed specifications. After completing the design, drawings were exported to ensure accurate laser cutting and fabrication. A laser cutting machine was then used to cut and engrave the MDF parts to specification, per the SolidWorks design. Once the components have been cut, the housing is assembled using cross-jointing and screws to ensure structural integrity and secure the parts in place.

The housing features several openings: (1) to allow airflow into the $PM_{2.5}$ particle sensor, (2) to accommodate the GPS antenna for satellite signal reception, and (3) for the display screen placement. Subsequently, tests were conducted to verify that the housing fits the devices and meets the design and functionality requirements established in SolidWorks. This design is experimental and requires optimization to serve as a prototype, potentially leading to the future commercialization of equipment. It is essential to adhere to electrical safety standards to protect electrical devices installed outdoors. This enclosure is moisture-proof (IP65), sunscreen-protected, and anti-corrosion, providing additional security against weather-related environmental hazards. The mobile devices (MD) house circuits C1 and C2 for conducting georeferenced pedestrian measurements were integrated into an MDF housing.

2.3 Mobile Devices (MD) Comparison

To evaluate reproducibility and test the MD's autonomy, simultaneous $PM_{2.5}$ measurements were conducted under stable conditions using four MDs. In addition to theoretical calculations of each circuit's consumption, physical tests were conducted in which each MD was connected to a 6V, 4A battery to assess performance and autonomy. The correlation between the $PM_{2.5}$ measurements from the different MDs was also analyzed using standard statistical methods.

2.4 Measurements at the Reference Site

Two SD were placed at the "Las Ninfas" (NIN) monitoring station, positioned just below the air sampling inlets of the reference sensors. The purpose of such measurements is to generate data for calibrating the measurement devices. Hourly $PM_{2.5}$ measurements from the NIN reference site and the SD were collected over two months and compared. A multiple linear regression analysis was performed to adjust the $PM_{2.5}$ values measured by the SD to the reference site measurements. The authorities of the Puebla Environmental Secretariat granted access to the NIN site facilities. The parameters derived from the linear regression model, which is formed using $PM_{2.5}$ from SD and temperature and humidity measurements from the NIN site, facilitate data calibration. These parameters are subsequently applied to the on-foot measurements conducted with the Mobile Device (MD) to enhance the accuracy and reliability of the readings. The mean absolute error (MAE) is calculated to evaluate the difference between the reference data and the calibrated model results.

2.5 Mobile Pedestrian Measurements

Georeferenced mobile pedestrian measurements were conducted in the streets and avenues of the historic center of Puebla using calibrated MD. These measurements were taken during the daytime (11 AM) and the evening (3 PM). These times were selected because they correspond to peak activity periods in the historic center, characterized by high vehicle and pedestrian traffic as people commute to work or return home. The measurements were conducted along four specific routes (R1, R2, R3, and R4) that start and end at "Las Ninfas" (NIN) Park, as shown in Figure 2. Each pedestrian route takes approximately 45 minutes to walk. The routes were chosen to include various typical areas such as residential, commercial, and tourist zones. Factors such as vehicular flow, commercial activity, public transportation availability, and green areas were considered.

Route R1 allows for measurements in areas with significant vehicular traffic and commercial activity. Route R2 was selected to evaluate areas with high pedestrian flow and local businesses, which could influence air quality. In contrast, the R3 route allowed for measurements in areas near parks and green spaces. Finally, R4 included areas with cobblestone streets and various types of vehicular traffic. Photographic and video evidence were collected during all the walks to later correlate sudden increases in $PM_{2.5}$ concentrations to emission sources.

The data cleaning process generated the following outputs: (i) maps of roadway concentrations, (ii) time series plots of concentrations, and (iii) a frequency analysis of peak $PM_{2.5}$ concentrations by emission source. These

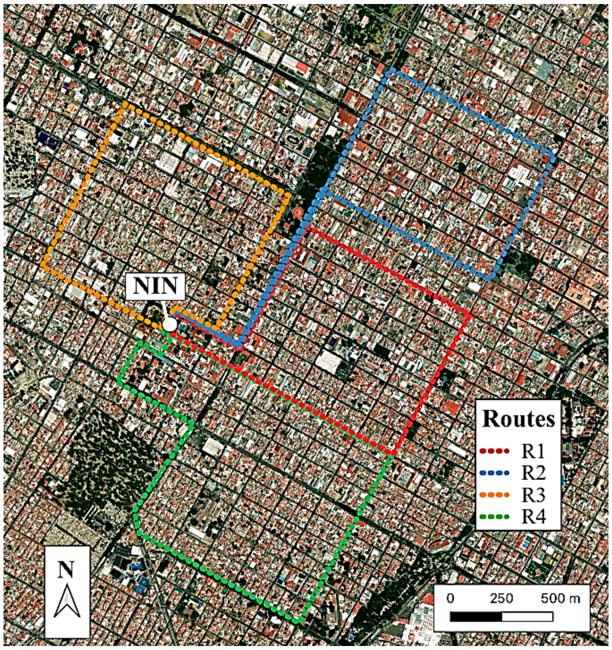

Figure 2. Map of downtown Puebla and collection data routes (R1, R2, R3, and R4), all of which started and ended at the "Ninfas" (NN) monitoring site.

analyses provide valuable information for informed decision-making. They enable the identification of areas with high particulate matter concentrations along avenues, enabling targeted pollution control efforts, policies, and actions to improve air quality in affected urban areas.

3. Results and discussion

3.1 $PM_{2.5}$ Sensor Wiring Diagrams

The SD used to compare with the reference site is integrated into a single circuit, "C1," as shown in Figure 3(a). This figure shows a schematic of the connections between the sensors (MicroSD, DHT11, RTC DS3231, SDS011, and LCD) and the development board (Arduino UNO).

The MD used for on-foot measurements consists of C1 and C2 circuits. The C2 circuit incorporates a GPS module that provides real-time georeferenced data, which is displayed on a screen and stored on a Micro SD card along with the registration date. The data logging date is synchronized between C1 and C2, enabling seamless integration of both databases. Figure 3 (b) shows a schematic of the connections for C2.

The circuits were housed in Static Devices (SD) for reference-site measurements and in Mobile Devices (MD) for on-foot measurements, as shown in Figure 4.

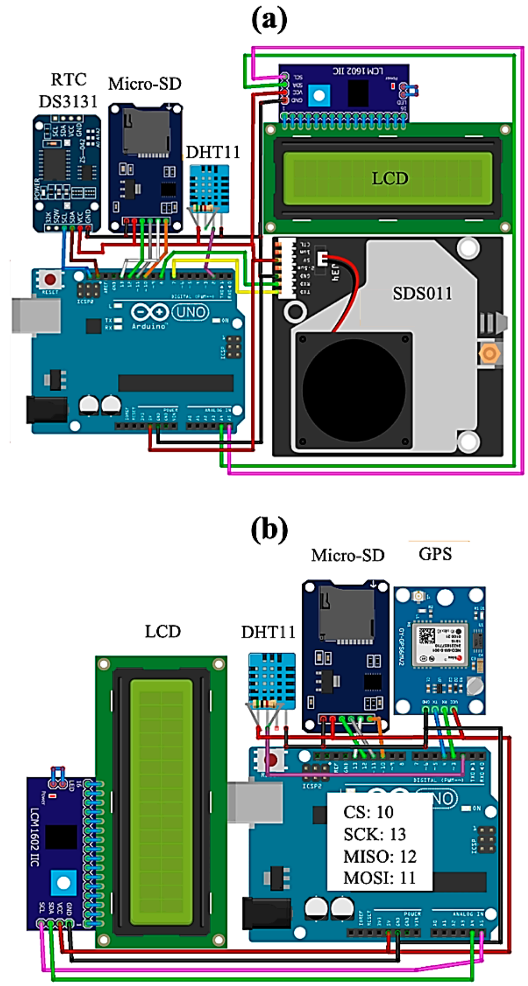

Figure 3. Circuit diagram of circuits: (a) C1 and (b) C2.

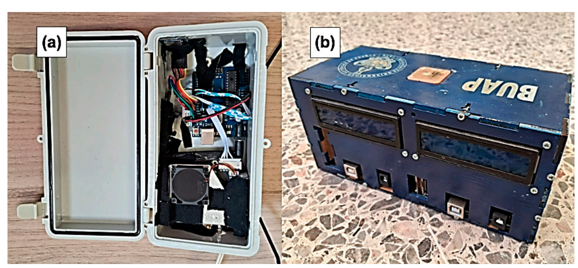

Figure 4. Image of (a) Static Devices (SD) for reference site measurements and (b) Mobile Devices (MD) for on-foot measurements.

3.2 Reproducibility and Intercomparison of Measurements with MDs

Figure 5 shows the placement of battery-powered MDs for simultaneous $PM_{2.5}$ measurements.

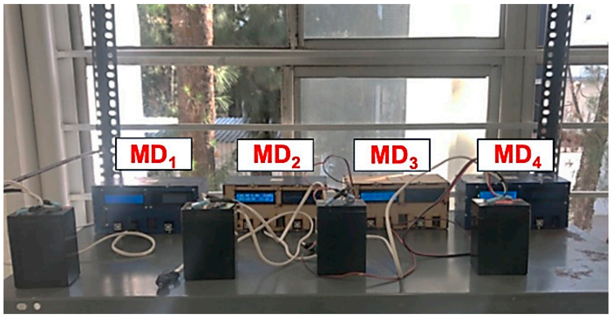

Figure 5. Simultaneous $PM_{2.5}$ measurements were performed using the MDs placed in a stable environment inside the University of Puebla.

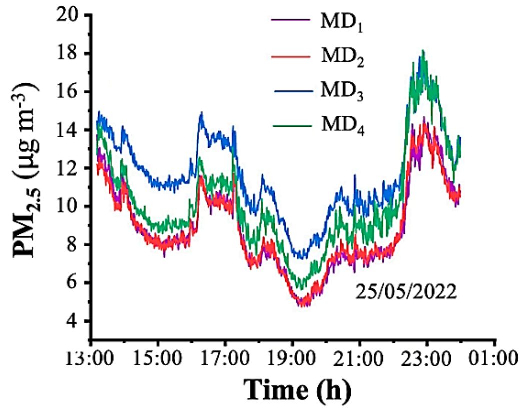

Figure 6. Time series of $PM_{2.5}$ concentrations using MD_1, MD_2, MD_3 and MD_4.

Figure 6 shows the temporal variation of $PM_{2.5}$ concentrations (mg m^{-3}) obtained with the four MDs. The four devices operate similarly; they respond with the same accuracy to sudden changes in $PM_{2.5}$ concentrations. The measurements are practically the same if the uncertainty (±15%) provided by the manufacturer is considered.

Figure 7 illustrates the correlation between the MD measurements. The ratio shown in 7(a) between MD_1 and MD_2 is highly consistent, with a correlation close to unity (0.96). Figure 7(a)-(e) shows that the ratios are generally above the 1:1 line, except for the MD3-MD4 ratio, which shows the opposite trend. In some cases, such as Figures 7(c) and 7(e), the linear fit shows that as particle concentration increases, the differences between sensor measurements also increase. However, this is not definitive, as Figures 7(a), 7(b), and 7(d) show fits that are almost parallel to the 1:1 line. According to the performance tests, the MD operates effectively for less than 4 hours, which is sufficient to complete mobile on-foot measurements lasting less than one hour.

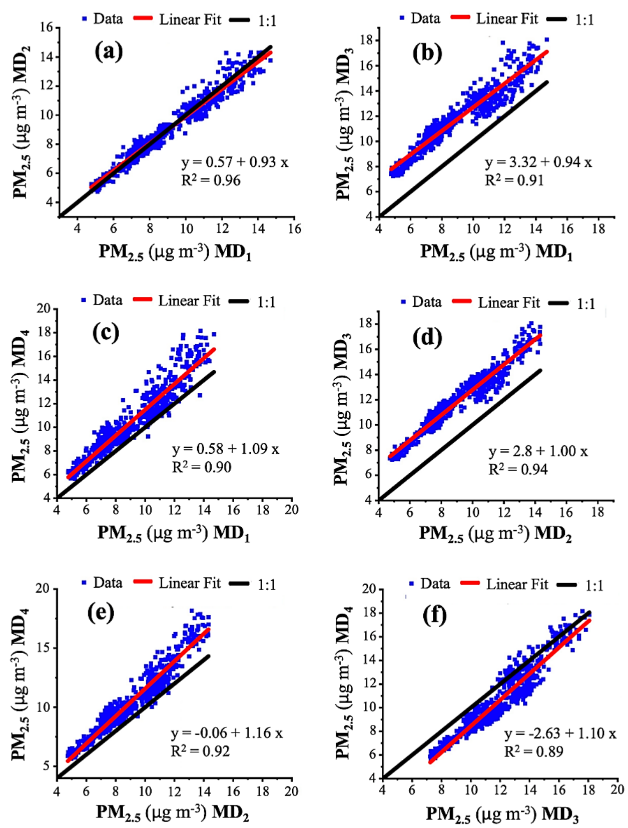

Figure 7. Correlation between mobile devices (MD). The black line represents a 1:1 ratio, and the red line represents the linear fit to the MD correlation.

3.3 Battery Autonomy Time

The battery discharge time for C1 and C2 is as follows:

$$\mathrm{td}_{\mathrm{C1}} = \frac{4\mathrm{Ah}}{0.1\mathrm{A}} = 40\mathrm{h} \quad (1)$$

$$\mathrm{td}_{\mathrm{C2}} = \frac{4\mathrm{Ah}}{0.0954\mathrm{A}} = 42\mathrm{h} \quad (2)$$

As a result, the battery in C1 lasts 40 h and powers the static device SD and an LCD screen. For C2, the battery lasts 42 hours, which, when combined with the SD and an LCD screen, forms the mobile device MD. These calculations assume the use of separate batteries for each circuit. Alternatively, a single battery could power the entire MD, providing approximately 20.5 hours of discharge time (6V, 4A battery). However, it is important to note that during actual measurements, the discharge time may be slightly less due to various factors. Additionally, the system draws 50 mA in idle state. Given this information, there is no issue with using the MD for monitoring, as the time required to complete the pedestrian routes in a day is less than 4 hours.

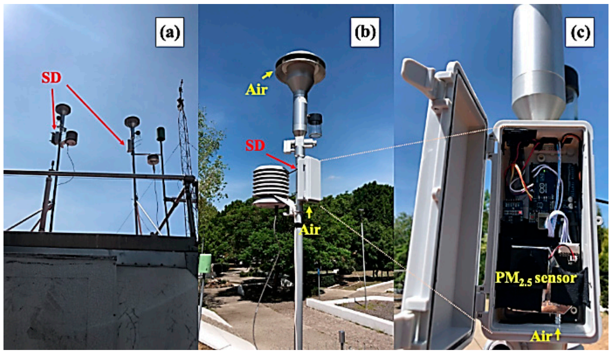

Figure 8. Static device (SD) placed next to the reference instruments at the *Las Ninfas* site (NIN).

3.4 Reference Site Measurements

Figure 8 (a)-(b) shows the placement of the SD just below the air inlet of the "Las Ninfas" (NIN) reference monitor. Figure 8(c) shows the interior of the SD equipped with the $PM_{2.5}$ LCS, the storage module, and the temperature and humidity sensors.

A multiple linear regression analysis is performed to fit the LCS data for particulate matter assembled at the SD to the reference-site data. Figure 9 shows the time series of $PM_{2.5}$ from (a) July 13 to July 17, (b) July 17 to July 21, (c) July 26 to July 29, and (d) July 29 to August 2, 2022.

The fit of $PM_{2.5}$ concentrations showed a moderate correlation with the reference data (R2 = 0.61, RMSE = 7.3 mg m^{-3}). The MAE of the $PM_{2.5}$ regression model is between 4.9 and 5.2 g m^{-3}, depending on the period of calibration, which agrees with the MAE interval of 1.9 to 8.4 g m^{-3} for SPS30, SD011, and OPC-N3, respectively, reported by Hofman et al. (2022). This comparison is appropriate, given that the $PM_{2.5}$ concentrations in that study are like those in this paper (< 20 mg m^{-3}). Although the calibrated LCS derived from this study provides valuable insights, it achieves only a moderate level of performance compared with others' reports. Table 1 summarizes the main features (price and model) of different calibrated low-cost sensors (LCSs) reported in the literature, highlighting the achieved accuracy and the calibration algorithms used.

3.5 Mobile Measurements

The $PM_{2.5}$ mobile measurements along the routes have standard deviations of 3.26 µg m^{-3}. Morning routes have an average $PM_{2.5}$ level (12.17 µgm^{-3}), similar to that of the afternoon (11.61 µgm^{-3}), and in both cases, the calibrated MD underestimates the reference values; the bias is slightly lower during the afternoon (-5.08) than during the day (-5.47). Figure 10 shows a map of the spatial distribution of the measurements and their correlation with the time series of $PM_{2.5}$ concentrations for route R1 on July 14, 2022.

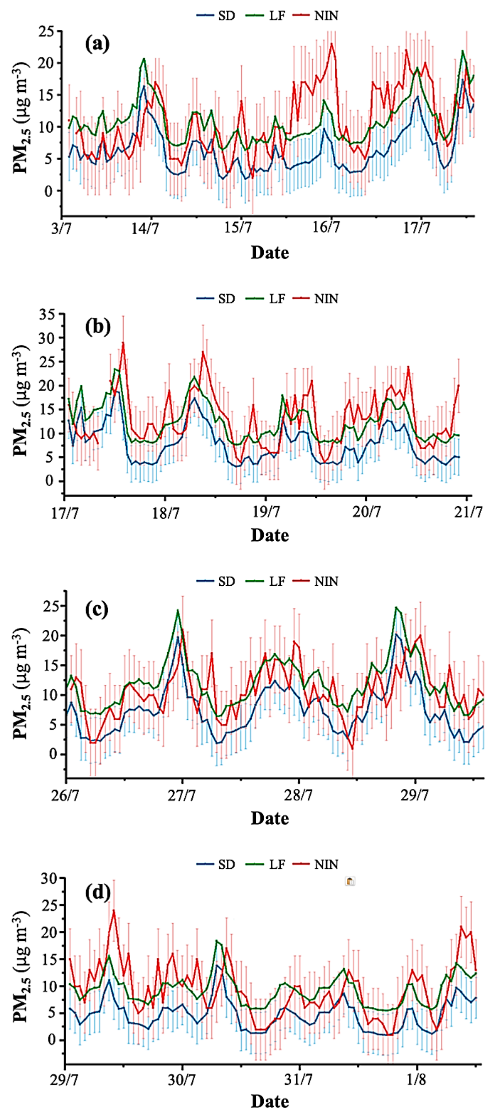

Figure 9. Time series of $PM_{2.5}$ concentrations with static devices (SD) and corresponding reference data from the NIN site. The green line represents the fit of $PM_{2.5}$ concentrations after calibrating with multiple linear regression (LF) for periods (a) July 13 to July 17, (b) July 17 to July 21, (c) July 26 to July 29, and (d) July 29 to August 2, 2022. The whiskers represent one standard deviation.

Likewise, photographs and videos captured during the routes were used to identify $PM_{2.5}$ sources. This identification process was complemented by a comparative analysis of maps showing hot spots and graphs depicting measurement data. The highest recorded peaks for each route (R1-R4) on the morning and evening routes were documented and attributed to specific emission sources, as detailed in Table 2.

Table 1. Summary of parameters to compare different calibrated LCS $PM_{2.5}$ results.

Make and Model	Cost (USD)	RMSE (mg m^{-3})	R^2	Calibration Method
Alphasense OPC-N3	~ 500	10.6		[(a)]LRM + Optimization
iPlug AM100	-	7.06	0.88	[(b)]LRM (T + RH)
TPI Sniffer4D	-	7.85	0.87	[(b)]LRM (T + RH)
Plantower PMS7003	12	1.03	0.83	[(c)]LRM (RH)
Plantower, PMS 5003	26	-	0.67	[(d)]MLRM
Nova Fitness, Alphasense, Sensirion, SDS011, OPC-N3, SPS30.	26-60	-	0.83-0.92	[(d)]MLRM + Optimization

[(a)] Kaur & Kelly, 2023, [(b)] Kang & Choi, 2024, [(c)]Aix et al., 2023, [(d)]Si et al., 2020, [(e)]Hofman et al., 2022.

Table 2. Frequency of occurrence of $PM_{2.5}$ sources associated with locations where recurrent increases in particulate matter measurements were observed.

Route	Number of Sources				
	V	N	C	R	BB
R1	838	337	183	526	19
R2	1027	303	211	317	35
R3	851	382	191	482	0
R4	956	238	269	338	0
Total	3672	1260	854	1663	54

VN = Vehicles; N = Natural, C=Crossing, R = resuspension; BB = Biomass burning

Motor vehicles are the predominant source of emissions in pedestrian areas (51%). We have identified two scenarios that occur at crosswalks: (*i*) When pedestrians wait at crosswalks, vehicles accumulate while awaiting a traffic light change, often positioning themselves within proximity (< 2m) to the pedestrians. In these instances, diesel vehicles are the primary contributors to emissions; (*ii*) In the second scenario, pedestrians wait at crosswalks while vehicles drive at low speeds on poorly maintained or cobblestone streets, not only the generation of $PM_{2.5}$ emissions, but also in the resuspension of dust from the

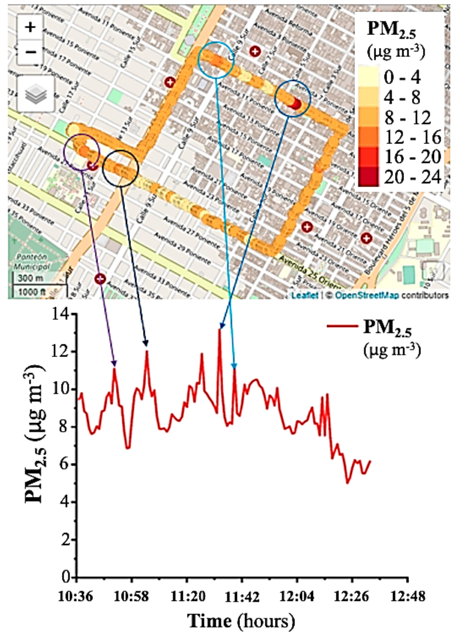

Figure 10. Hot spots map and diurnal variation of $PM_{2.5}$ (±3.2) along R1 route (morning) on July 14, 2022.

ground, accounting for 21%. The sources of biomass burning identified include small, fixed, or itinerant businesses such as rotisseries or establishments that use firewood as fuel. These sources were relatively scarce and were primarily located near downtown (0.7%). Additionally, other significant sources of particulate matter were found near green areas such as natural parks. These open spaces, which allow for greater wind flow, act as collectors of dust, pollen, and other particulate matter, thereby contributing to the recorded measurements, accounting for 15.9%.

4. Concluding Remarks

This study demonstrated the feasibility of utilizing Low-Cost Sensor (LCS) technology to develop calibrated devices for monitoring pedestrian exposure to $PM_{2.5}$. Specifically, these devices facilitate (i) the measurement of PM2.5 exposure for pedestrians, (ii) the identification of areas with high particulate levels during their routes, and (iii) the detection of sources contributing to elevated $PM_{2.5}$ levels in downtown Puebla. Two types of circuits were developed. When used together, they form a mobile device (MD). For the static device (SD), circuit C1 was modified by removing the LCD screen. Both devices were equipped with sensors for PM2.5, temperature, relative humidity, GPS, timers, MicroSD storage modules, and displays for real-time data visualization. They were programmed on an ATmega328P microcontroller using an Uno board, which operates at 16 MHz and has 32 KB of Flash memory and 2 KB of RAM. The Uno board also features 14 digital pins, 6 analog pins, and serial and USB communication ports. The MD was housed in a medium-density fiberboard (MDF) casing, while the SD required an IP65-rated enclosure to ensure waterproofing and protection from physical damage.

Inter-comparison tests showed an average Pearson correlation coefficient of 0.93 among the devices, indicating consistent measurement behavior for PM2.5 concentrations. Measurement discrepancies were attributed to a ±15% margin of error. Circuit C1 consumed 0.1 A, and circuit C2 consumed 0.0954 A, allowing battery-powered circuits to operate for up to 40 or 20 hours using a single battery per circuit. Calibration using a multiple linear regression model yielded a moderate adjustment accuracy (MAE = 5.0; RMSE = 7.3 mg) for the device readings compared to data from the "Las Ninfas" monitoring station. This level of accuracy, though somewhat uncertain, is comparable to that of other low-cost commercial sensors operating under similar PM2.5 concentrations (Hofman et al., 2022). The device is suitable for use in environments with humidity levels not exceeding 90%, but calibration should be tailored to specific environmental conditions. For future studies, it is recommended to conduct a sensor training period, involving measurements over at least 3 months across multiple locations, to improve confidence in readings from low-cost sensors.

The results of this experiment are not directly applicable to other seasons (Kang & Choi, 2024). It should be emphasized that the experiment was conducted during the rainy season in Mexico (June-September), which provides information on the lower bound of $PM_{2.5}$ concentrations to which pedestrians could be exposed. If the experiment were conducted at another time of year, in addition to the usual sources, which would be similar at other times of the year, we would also have to add higher background ambient concentrations and a greater amount of dust in streets and avenues during the hot-dry season (March to May) and similarly during the cold-dry season (December to February). For this reason, it is essential to conduct similar experiments at other times of the year. The accuracy of measurement devices based on LCS increases as particle size decreases, a relationship related to airflow rate entering the devices and humidity (Kaur & Kelly, 2023). The SDS011 low-cost sensor used in this experiment measured both $PM_{2.5}$ and PM_{10} concentrations; however, we found that PM_{10} concentrations showed poor correlation with the reference measurements, and the linear regression model was insufficient to significantly reduce the gap between the experimental and reference measurements. In this regard, only $PM_{2.5}$ was used. On the other hand, more recent LCS (e.g., SEN55) measure ultrafine particulates ($PM_{1.0}$) and NOx, whereas SDS011 is limited to coarse and fine particulate matter. This study was the first to measure pedestrian exposure to visitors to the historic center of Puebla. However, we are currently expanding the scope of the experiment to include measurements of ultrafine particles ($PM_{1.0}$) and considering different heights to differentiate between children and adults.

Survey data from Puebla's historic center identified motor vehicles as the primary source of sudden $PM_{2.5}$ spikes (57%), followed by particle resuspension (21%), natural sources (15.9%), road crossings (10.8%), and biomass burning (0.7%). Areas with cobblestone intersections or narrow streets experienced frequent increases in $PM_{2.5}$ concentration. To reduce particulate emissions, public transportation routes should avoid unpaved roads and cobblestone surfaces. Additionally, in areas where pedestrians wait at traffic lights, maintaining a distance of at least 1.5 meters from vehicles is recommended to minimize exposure risk. Future studies should include continuous $PM_{2.5}$ measurements at crosswalks at different heights to assess personal exposure across age groups.

Acknowledgements

The authors wish to thank all undergraduate students from the "Delfin" program who participated in the field experiment. granted. Additionally, thanks are extended to the Secretary of the Environment of the State of Puebla for the facilities provided to install the ED at the NIN site.

Funding

This study was supported by the BUAP-IPN consortium project, as the main author received sponsorship from project 001-VIEPIPN2024 to conduct the research reported in this manuscript.

Conflict of Interest

The authors have no conflicts of interest to declare.

References

Adhiwibowo, W., Daru, A. F., & Hirzan, A. M. (2020). Temperature and humidity monitoring using DHT22 sensor and Cayenne API. *Jurnal Transformatika*, *17*(2), 209-214.
https://doi.org/10.26623/TRANSFORMATIKA.V17I2.1820

Aix, M. L., Schmitz, S., & Bicout, D. J. (2023). Calibration methodology of low-cost sensors for high-quality monitoring of fine particulate matter. *Science of the Total Environment*, *889*, 164063.
https://doi.org/10.1016/J.SCITOTENV.2023.164063

Akinwole, O. O., Oladimeji, T. T. (2018). Design and Implementation of Arduino Microcontroller Based Automatic Lighting Control with I2C LCD Display. *J Electr Electron Syst*, *7*, 258.
https://doi.org/10.4172/2332-0796.1000258

Badura, M., Batog, P., Drzeniecka-Osiadacz, A., & Modzel, P. (2018). Evaluation of Low-Cost sensors for ambient PM2. 5 monitoring. *Journal of Sensors*, *2018*(1), 5096540.
https://doi.org/10.1155/2018/5096540

Cromar, K. R., Duncan, B. N., Bartonova, A., Benedict, K., Brauer, M., Habre, R., ... & Volckens, J. (2019). Air pollution monitoring for health research and patient care. An official American Thoracic Society workshop report. *Annals of the American Thoracic Society*, *16*(10), 1207-1214.
https://doi.org/10.1513/ANNALSATS.201906-477ST

DeSouza, P., Anjomshoaa, A., Duarte, F., Kahn, R., Kumar, P., & Ratti, C. (2020). Air quality monitoring using mobile low-cost sensors mounted on trash-trucks: Methods development and lessons learned. *Sustainable Cities and Society*, *60*, 102239.
https://doi.org/10.1016/J.SCS.2020.102239

Feenstra, B. J. (2020). *Development of Methodologies for the Use and Application of Air Quality Sensors to Enable Community Air Monitoring* (Doctoral dissertation, University of California, Riverside).
https://escholarship.org/uc/item/0659j8sn.

Gao, M., Cao, J., & Seto, E. (2015). A distributed network of low-cost continuous reading sensors to measure spatiotemporal variations of PM2. 5 in Xi'an, China. *Environmental pollution*, *199*, 56-65.
https://doi.org/10.1016/J.Envpol.2015.01.013

Hofman, J., Nikolaou, M., Shantharam, S. P., Stroobants, C., Weijs, S., & La Manna, V. P. (2022). Distant calibration of low-cost PM and NO2 sensors; evidence from multiple sensor testbeds. *Atmospheric Pollution Research*, *13*(1), 101246.
https://doi.org/10.1016/j.apr.2021.101246

Kang, J., & Choi, K. (2024). Calibration methods for low-cost particulate matter sensors considering seasonal variability. *Sensors*, *24*(10), 3023.
https://doi.org/10.3390/S24103023

Kaur, K., & Kelly, K. E. (2023). Performance evaluation of the Alphasense OPC-N3 and Plantower PMS5003 sensor in measuring dust events in the Salt Lake Valley, Utah. *Atmospheric Measurement Techniques*, *16*(10), 2455-2470.
https://doi.org/10.5194/amt-16-2455-2023

Khreis, H., Johnson, J., Jack, K., Dadashova, B., & Park, E. S. (2022). Evaluating the performance of low-cost air quality monitors in Dallas, Texas. *International journal of environmental research and public health*, *19*(3), 1647.
https://doi.org/10.3390/ijerph19031647

Lee, C. H., Wang, Y. B., & Yu, H. L. (2019). An efficient spatiotemporal data calibration approach for the low-cost PM2. 5 sensing network: A case study in Taiwan. *Environment international*, *130*, 104838.
https://doi.org/10.1016/J.ENVINT.2019.05.032

Liu, H. Y., Schneider, P., Haugen, R., & Vogt, M. (2019). Performance assessment of a low-cost PM2. 5 sensor for a near four-month period in Oslo, Norway. *Atmosphere*, *10*(2), 41.
https://doi.org/10.3390/ATMOS10020041

Liu, X., Jayaratne, R., Thai, P., Kuhn, T., Zing, I., Christensen, B., ... & Morawska, L. (2020). Low-cost sensors as an alternative for long-term air quality monitoring. *Environmental research*, *185*, 109438.
https://doi.org/10.1016/J.ENVRES.2020.109438

Nothhelfer, M., Sperber, O., Todea, A. M., Schunke, B., Romazanowa, O., Schumacher, S., ... & Asbach, C. (2023). Effect of an aerosol dryer on ambient PM measurements with SDS011 low cost sensors during a two-year period in Duisburg, Germany. *Aerosol and Air Quality Research*, *23*(10), 230080.
https://doi.org/10.4209/aaqr.230080

Omidvarborna, H., & Kumar, P. (2024). Low-cost sensors for air quality monitoring. In *Reference Module in Earth Systems and Environmental Sciences*. Elsevier.
https://doi.org/10.1016/B978-0-323-99762-1.00046-2

Pang, X., Chen, L., Shi, K., Wu, F., Chen, J., Fang, S., ... & Xu, M. (2021). A lightweight low-cost and multipollutant sensor package for aerial observations of air pollutants in atmospheric boundary layer. *Science of the Total Environment*, *764*, 142828.
https://doi.org/10.1016/J.SCITOTENV.2020.142828

Raysoni, A. U., Pinakana, S. D., Mendez, E., Wladyka, D., Sepielak, K., & Temby, O. (2023). A review of literature on the usage of low-cost sensors to measure particulate matter. *Earth*, *4*(1), 168-186.
https://doi.org/10.3390/earth4010009

Si, M., Xiong, Y., Du, S., & Du, K. (2020). Evaluation and calibration of a low-cost particle sensor in ambient conditions using machine-learning methods. *Atmospheric Measurement Techniques*, *13*(4), 1693-1707.
https://doi.org/10.5194/AMT-13-1693-2020

Thangavel, P., Park, D., & Lee, Y. C. (2022). Recent insights into particulate matter (PM2. 5)-mediated toxicity in humans: an overview. *International journal of environmental research and public health*, *19*(12), 7511.
https://doi.org/10.3390/IJERPH19127511

WMO (2024). Integrating low-cost sensor systems and networks to enhance air quality applications. World Meteorological Organization. GAW Report No. 293, 182 pp.

Ye, Z., Jiang, X., & Wang, Z. (2012). Measurements of particle size distribution based on mie scattering theory and markov chain inversion algorithm. *J. Softw.*, *7*(10), 2309-2316.